Phys. Med. Biol. **44** (1999) 75–86. Printed in the UK PII: S0031-9155(99)95844-X

Determination of the object surface function by structured light: application to the study of spinal deformities

M Buendía†‡, R Salvador†, R Cibrián†, M Laguia§ and J M Sotoca†

† Biofisica y Física Médica, Dpt. de Fisiología, Facultad de Medicina y Odontología, Universidad de Valencia, Spain

§ Traumatología y Ortopedia, Dpt. de Cirugía, Facultad de Medicina y Odontología, Universidad de Valencia, Spain

Received 8 July 1998, in final form 21 September 1998

Abstract. The projection of structured light is a technique frequently used to determine the surface shape of an object. In this paper, a new procedure is described that efficiently resolves the correspondence between the knots of the projected grid and those obtained on the object when the projection is made. The method is based on the use of three images of the projected grid. In two of them the grid is projected over a flat surface placed, respectively, before and behind the object; both images are used for calibration. In the third image the grid is projected over the object. It is not reliant on accurate determination of the camera and projector pair relative to the grid and object. Once the method is calibrated, we can obtain the surface function by just analysing the projected grid on the object. The procedure is especially suitable for the study of objects without discontinuities or large depth gradients. It can be employed for determining, in a non-invasive way, the patient's back surface function. Symmetry differences permit a quantitative diagnosis of spinal deformities such as scoliosis.

1. Introduction

Structured light has often been used as a means for drawing three-dimensional information about a setting from a monocular image, thus obtaining either a depth map or a series of 3D co-ordinates of the field points observed (Kak 1985, Vuylsteke and Oosterlinck 1990, Lindsey and Blake 1994, Busboom and Schalkoff 1996, Hartrumpf and Munser 1997). This can be considered a particular case of stereoscopic vision in which one of the two cameras is replaced by a known vision pattern that is projected onto the scene. From the deformation of such a pattern when falling onto the objects in the scene, the 3D positions of the surface points of the objects can be inferred. Numerous problems in robotics (Will and Pennington 1971, Kak 1985) and medicine (Arffa *et al* 1989, Windecker and Tiziani 1995) have been satisfactorily resolved through structured light patterns.

Different procedures (Agin and Binford 1973, Posdamer and Altschuler 1982, Sörgel and Schalkoff 1997) have been proposed in order to infer the surface shape of the objects based on the appearance of the light projection on the objects in the scene. In most cases, the problem is the ambiguity in the identification of the projected lines, which some authors (Boyer and Kak 1987, Vuylsteke and Oosterlinck 1990) have come to call the 'indexing problem', namely the difficulty in linking each line detected in the image to its position in the projected structure.

‡ Address for correspondence: M Buendía Gómez, Biofísica y Física Médica, Facultad de Medicina y Odontología, Av. Blasco Ibáñez, 15, 46010-Valencia, Spain. E-mail address: buendiag@uv.es

0031-9155/99/010075+12$19.50

Once the indexing problem is resolved, the depth in the points in the scene can be calculated through triangulation.

One of the first procedures used in the resolution of fringe identification was the binary coding of light fringes (Yang *et al* 1984). The fringe pattern is projected several times, each time with a binary code that determines a 1 or 0 status for specific fringes. Thus, with $\log 2N$ different projections, the scene can be lit up with $N - 1$ unequivocally indexed fringes. To a great extent, this reduces the number of projections with regard to single fringe sweeping, although it is tedious, subject to error, and one cannot work with objects that may drift slightly between the projections.

Fringe-colour based coding is another approach (Bayer and Kak 1987). This method requires one projection only. A series of fringes are coded with different amounts of red, green and blue in a way that the signals corresponding to these three colours can be analysed independently, thus achieving the identification of the fringe number by means of its colour. A simpler version of this technique, less powerful but inexpensive, is intensity level coding (Carrihill and Hummel 1985). The effects of the reflectance variation can be overcome by using additional light patterns.

Finally, we must outline the light pattern binary coding approach (Vuylsteke and Oosterlinck 1990). The pattern consists of black and white dotted areas specifically arranged so that each area can be identified through the unique arrangement of the bitmap of the projected coding. Such arrangements will not vary due to perspective effects, and therefore this can be considered a robust system. Its major problems stem from the difficulty in obtaining good spatial resolution and the susceptibility of the image-acquisition process to create artefacts, due to the interference caused by the textures in the projection of a light pattern made up of thousands of tiny dots.

This paper presents a structured light approach to determine object surface functions. Unlike other structured light methods, our approach solves the indexing problem on a square grid, based on a previous calibration method that is suitable for continuous surfaces. Surfaces should also be 'smooth', i.e. the spatial frequency of surface undulation is less than the stripe frequency. The approach enables us to determine the object surface function without taking into account the geometry between camera and projector, and to avoid the determination of the camera image plane position. The procedure has been applied to the determination of the back surface function in order to assess its usefulness in establishing the degree of scoliosis and other pathologies associated with spine malformation.

2. Theoretical basis and experimental device

The proposed procedure for the determination of the surface function of an object is based on the analysis of the deformation experienced by a square grid (figure 1(*a*)) when projected on a non-flat surface (object grid) (figures 1(*b*), (*c*)).

In order to establish the deformation, and in addition to the object grid, the procedure requires the recording of the images of the grid projected on a flat surface (screen) placed, respectively, behind the object (back grid), and in front of the object (front grid). The experimental set-up (figure 2) indicates the position of the screen for obtaining the three images needed for the development of the method. The image plane of the camera must be parallel to the back and front reference planes.

The position of the screen, when it is placed behind the object, will be used as the origin of the distances in the calculation of the object thickness in each surface point. The comparison between back grid and front grid avoids having to consider the grid projection geometry. We can establish the propagation straight lines of the light beams according to the different

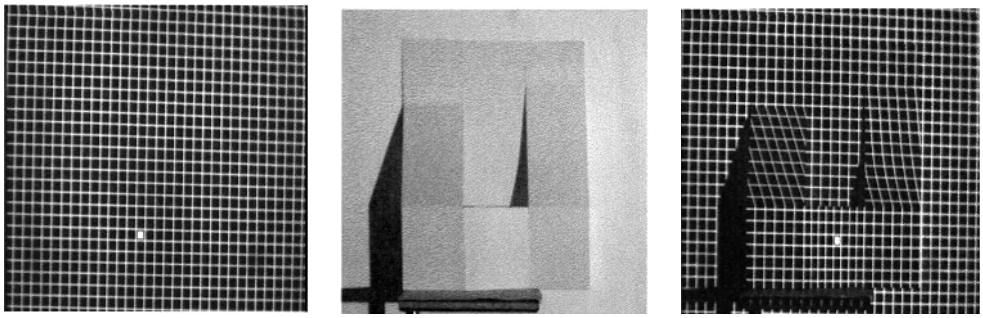

(*a*) (*b*) (*c*)

Figure 1. Image captured by the CCD, corresponding to (*a*) the projected grid on the screen placed behind the object (back grid), (*b*) object test and (*c*) the projected grid on the object (object grid).

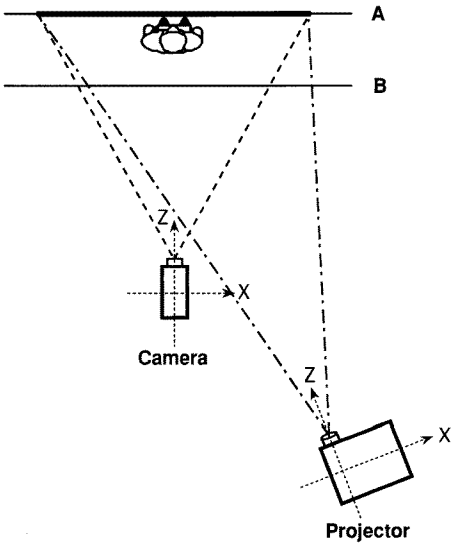

Figure 2. Experimental set-up used in grid projection and image capture. Screen position: A for the back grid and object grid, B for the front grid.

locations of the knots (line crossings in the grid) in the two screen positions. The object grid and the back grid only differ in the zone occupied by the object, this permitting us to obtain the distance between the back plane and the object surface points (surface function) as per the following approach.

If any light beam coming from the focus (projector objective) is considered (figure 3), the points of the straight line crossing the front plane, the object surface and the back plane correspond, respectively, to positions $r_2(x_2, y_2)$, $r_3(x_3, y_3)$ and $r_1(x_1, y_1)$. The camera gets the three point images aligned on the image plane ($rp_2(xp_2, yp_2)$, $rp_3(xp_3, yp_3)$ and $rp_1(xp_1, yp_1)$).

Due to purely geometrical reasons relative to figure 3 (appendix 1), z (the value of the surface function in that particular object point) can be drawn in relation with rp_1, rp_2 and rp_3:

$$z = Dk(rp_3 - rp_1)/[(k-1)(rp_2 - rp_1) + (rp_3 - rp_1)] \tag{1}$$

where $k = (D + D_1 + D_2)/D$. This expression obtains the coordinate z for each image point

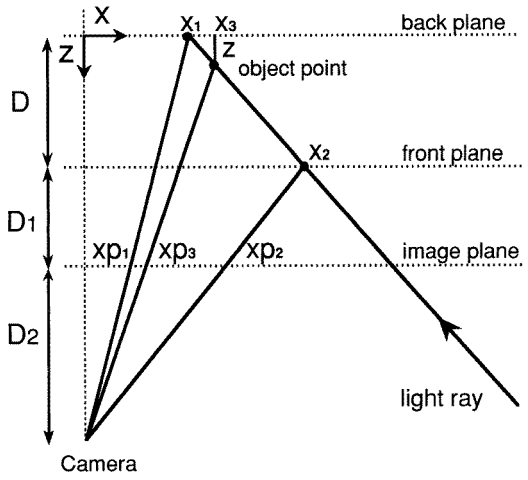

Figure 3. Geometry of the proposed procedure in the XZ plane. Representation of the x coordinate of the intersection points of a light beam with the planes: front (x_2), object (x_3) and back (x_1), and their corresponding representations on the camera's image plane (xp_2, xp_3, xp_1). D, D_1, and D_2 are the distances between the indicated points, and z is the distance from the object point to the back plane.

without having to know the projection geometry of the structured light, and independently from the units in which the distances on the image plane are measured; in our case they are pixels measured on the obtained images. We only need to know distance D between the back and front planes, as k can be drawn by comparing the back grid and front grid (appendix 1).

Since the distances appear in the z expression as differences with regard to one point in the image plane, the origin can be taken from any image point. Specifically, and as is common in digital images, we have taken the top left point, the OX axis, as the horizontal origin towards the right, and the OY axis as the vertical origin downwards.

Therefore, in the images of the front grid, back grid and object grid, we shall obtain the coordinates for each knot (step 3.4 of the next section). The correspondence will be established between the knots of the three grids, in other words the three positions held by the same knot of the projected grid will be determined (step 3.5 of the next section). And from the z expression the surface function will be drawn for each knot in the object image (step 3.6 of the next section).

3. Image processing

Specific software has been developed for the treatment of front grid, back grid and object grid images. To correctly establish the correspondence between the knots in the three images, a mark was made on the projected grid by inserting a square in one of the grid cells. The mark is therefore detectable in all the images.

The steps of the cited software are described below. The figures that illustrate these steps correspond to the test object used in the assessment of the accuracy of the proposed procedure. The test object is formed by three platforms with a z dimension of 1.0, 26.2 and 50.6 mm respectively joined by different slope planes (figure 1(*b*)).

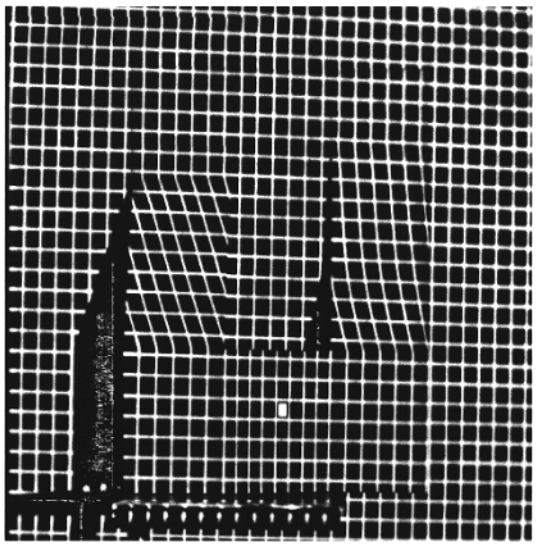

Figure 4. Object grid image after application of normalization process.

3.1. Pre-processing

Because of the inevitable variation of illumination of the different parts of the image, overall in the named object grid (figure 1(*c*)) it is not suitable to use a global normalization procedure for the whole image, so local normalization has been applied over the images directly captured by the camera. Our approach (Buendía *et al* 1997) consists of building two bidimensional functions $t_u(x, y)$ and $t_l(x, y)$ with the upper and lower reference threshold values respectively (see step A.1). These functions compute the local contrast-stretching function at each point (x, y) of the image (see step A.2).

Step A.1. The 512×512 pixel image is divided into 34×34 cells of 15×15 pixels, $g(x, y)$ being the grey level of each pixel. For each cell, j, $t_{u,j}$ and $t_{l,j}$ are 80% and 20% respectively of the accumulated histogram of grey levels of the cell pixels. These values are assigned to the central pixel (x_{0j}, y_{0j}) of the corresponding cell. For each image point, $t_u(x, y)$ and $t_l(x, y)$ are calculated by double-linear interpolation by use of the values corresponding to $t_{u,j}$ and $t_{l,j}$ for the four nearest cell centres.

Step A.2. After those functions have been computed for all pixels, one transforms the image by contrast stretching the histogram using a clipping procedure that assigns, to each pixel, a grey level $g'(x, y)$ from zero to $G_M = 255$ given by

$$g'(x_i, y_i) = \begin{cases} 0 & \text{if } g(x, y) \leqslant t_l(x, y) \\ G_M & \text{if } g(x, y) \geqslant t_u(x, y) \\ G_M[g(x_i, y_i) - t_l(x_i, y_i)] & \\ \quad /[t_u(x_i, y_i) - t_l(x_i, y_i)] & \text{if } t_l(x, y) < g(x, y) < t_u(x, y). \end{cases} \tag{2}$$

In the normalized image (figure 4), the mark is detected by looking for the point with the context having the highest number of pixels with a high grey level. The mark's centre position is registered and the mark is eliminated from the normalized image to facilitate the subsequent steps.

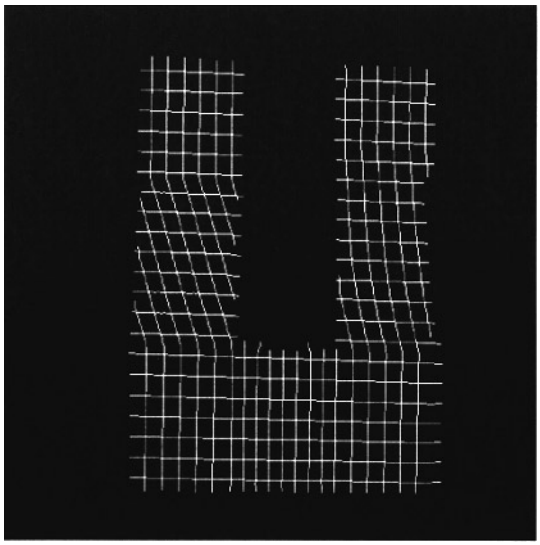

Figure 5. Binarized object grid image.

3.2. Object mask delimitation

This is not an essential step but it helps to speed up steps 3.5 and 3.6. By means of a polygonal line, the pixels that contain the object or the object interest zone can be selected in the object grid image.

3.3. Binarization and skeletonization

Once the images have been normalized, skeletonization of lines is carried out. Skeletonization is performed independently for the vertical and horizontal stripes. For the vertical (horizontal) lines the grey level of each row (column) pixel is recalculated as follows

$$g''(x, y) = 1/7 \sum_{i=-3}^{+3} g'(x, y + i) \qquad \left(g''(x, y) = 1/7 \sum_{i=-3}^{+3} g'(x + i, y) \right). \quad (3)$$

This softening minimizes the discontinuities due to the pixel effect. For each row (column) the $g''(x, y)$ function can be interpreted as separated intensity peaks located on the pixels corresponding to vertical (horizontal) lines. For each one of these peaks the maximum value is determined, and we made the grey level of this pixel to be 1. The grey level value of the rest of the pixels is considered as 0. The neighbouring pixels with grey level 1 are considered as elements of a vertical (horizontal) line. This algorithm is quite efficient in the recognition of the lines but sometimes discontinuities appear in them. A procedure to join the corresponding segments to form a complete line was devised. To avoid inadequate links between two segments, especially in the object image where the lines can be very close to each other, the acceptation of the operator is required to make some links.

With these considerations, two binary images are built, one with the vertical lines (slope greater than 1) and another with the horizontal lines (slope smaller than 1). The logical addition of these images provides a skeletonized image of the grid (figure 5).

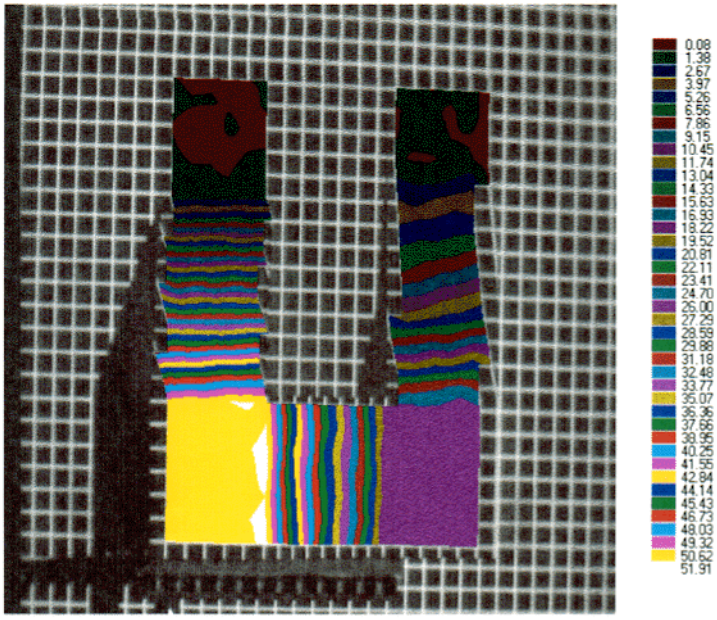

Figure 6. Surface function of test object, represented upon the original image. The scale indicates z values in mm.

3.4. Location of knots

A knot is the intersection of a vertical line with a horizontal one. Only one point can be considered as a knot between two lines. There are cases in which the geometry of vertical and horizontal lines makes more than one point to be considered as a knot. In such cases the mass centre of the possible knots is selected as the knot.

3.5. Correspondence between knots

As has been said in the pre-processing step, the mark's centre position in the three grid projections is known. This allows us to take one of the four knots around the mark centre as the knot (0,0) in the three images and from this knot to follow the skeletonized lines in the same direction in the three images to make the correspondence between the equivalent knots. This implies that the coordinates of rp_1, rp_2 and rp_3 for each knot are known. If a mask of the object has been made only the knots belonging to the object are considered in the procedure.

3.6. Calculation of surface function, z

Equation (1) is applied to each knot. For the rest of the pixels an interpolation is carried out. Firstly, the interpolation is made for the pixels on the lines, thus obtaining the corresponding z values. For the pixels out of the lines, a double interpolation is made taking into account the z values of the four nearest pixels in the four directions of the image plane. The array containing the value of z for each pixel of the object image is the object surface function (figure 6).

4. Materials and method

The experimental set-up is shown in figure 2. The projected grid is a slide obtained by photographing a square grid. The projector focal length used was 120.0 ± 0.5 mm which keeps the projected grid focused on both the front and back screen, and hence on the object. The pitch of the projected square grid on the back screen was between 10 and 35 mm, or even more, depending on the irregularities and size of the analysed object and the accuracy desired. The images were captured by a CCD video camera (Sony, SSC-MB70CE) and stored in the memory of a Pentium computer by a video digitizer board (Matrox, PIP-1024B) for subsequent analysis. The angle Φ between the Z-axes of the projector and the camera (figure 2) could be anything, but to achieve higher accuracy it should be between 30 and 45°, as will be shown in the next section. The CCD image plane may be parallel to the screens used for calibration. The distance between the camera and the object depends on the working volume and it should be chosen so that the whole object appears on the monitor screen. During the whole process the positions of the camera and the grid projector were not altered.

5. Results and discussion

5.1. Method sensitivity

The error associated with the determination of z could be evaluated taking into account that equation (1) represents a relationship between distances in the image plane:

$$z = Dkl_r/[(k-1)l_o + l_r] \tag{4}$$

where $l_r = (rp_3 - rp_1)$ and $l_o = (rp_2 - rp_1)$. The relative error of z ($\mathrm{Er}(z)$) can be obtained by derivation as follows:

$$\begin{aligned} \mathrm{d}z/z = {} & \mathrm{d}D/D + (l_r - l_o)/[(k-1)l_o + l_r]\,\mathrm{d}k/k + l_o(k-1)/[(k-1)l_o + l_r]\,\mathrm{d}l_r/l_r \\ & -l_o(k-1)/[(k-1)l_o + l_r]\,\mathrm{d}l_o/l_o. \end{aligned}$$

Taking into account that the relative error of all the distances in the image plane is the same and that errors must always be added, we can write

$$\mathrm{Er}(z) = \mathrm{Er}(D) + (l_r - l_o)/[(k-1)l_o + l_r]\,\mathrm{Er}(k) + 2l_o(k-1)/[(k-1)l_o + l_r]\,\mathrm{Er}(l) \tag{5}$$

where $\mathrm{Er}(l)$ represents the relative error of the distances measured on the image plane.

The error upper bound for z, taking into account that k is always greater than or equal to 1, could be written as follows:

$$\mathrm{Er}(z) = \mathrm{Er}(D) + \mathrm{Er}(k) + 2\,\mathrm{Er}(l). \tag{6}$$

The relative error of D is less than 0.4% because it is a length and can be measured with high precision. The relative errors of k and l depend on the design of the procedure itself. In this sense, in our error analysis, we have considered three types of errors: experimental set-up error, image processing error and calibration error, which are discussed below.

5.1.1. Experimental set-up error. This is associated with the projection angle, Φ and the arrangement of the experimental set-up. This angle may be anything between 0 and 90° but for low Φ values there are few differences between the positions rp_1, rp_2 and rp_3 and therefore a higher relative error in the distance measurement. On the other hand, for high projection angles (higher than 45°) other problems appear, such as:

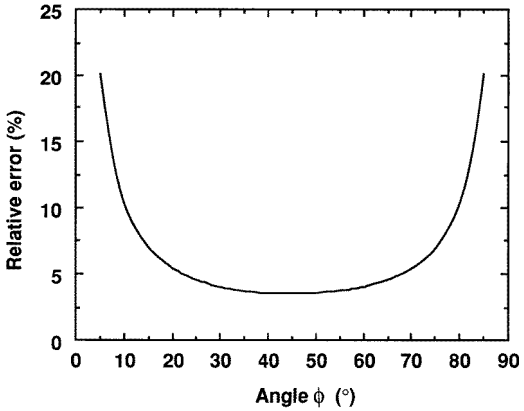

Figure 7. Influence of Φ angle projection on the relative error of the distances measured in the image plane.

(i) The mark used in establishing the correspondence between knots cannot appear in both back-grid and front-grid images because the projected mark appears further away from the field captured by the camera.

(ii) The grid projected under high angles presents a very different focus on the right and left sides.

To determine the optimum projection angle, the influence of Φ on the relative error of distances measured in the image plane $\mathrm{Er}(l)$ has been analysed. By geometric considerations, it can be written as

$$\mathrm{Er}(l) = \Delta\Phi / \cos\Phi \sin\Phi \tag{7}$$

where $\Delta\Phi$ is the absolute error in Φ. For $\Delta\Phi$ equal to 1°, the graph corresponding to equation 7 (figure 7) shows that the relative error drops for values of Φ up to 45° but the decrease is slow from 30°, the variation being between 7 and 4%.

All these considerations validate the above statement, i.e. that the projection angle, Φ, should be between 30 and 45°, which we have confirmed experimentally. Table 1 shows the determination of z for the test object for different values of Φ. In any case, table 1 also shows that the projection angle chosen is not a critical and determining value in the method, as the approximation obtained is quite good even for small angles.

Table 1. Depth values, z (mm), for the test object, for the indicated Φ projection angle values. The actual values of the analysed points are 50.6, 26.2, and 1.0 (mm).

10°	15°	20°	25°	30°	35°	40°	45°
49.3 ± 2.6	49.2 ± 1.3	49.9 ± 0.7	50.4 ± 0.8	50.8 ± 0.7	50.8 ± 0.6	50.4 ± 0.6	50.6 ± 0.6
27.2 ± 2.6	27.0 ± 2.2	26.7 ± 1.3	26.8 ± 1.3	26.0 ± 0.6	26.6 ± 0.6	26.9 ± 0.6	26.8 ± 0.6
1 ± 3	1.6 ± 1.3	1.1 ± 1.3	1.2 ± 1.3	1.2 ± 1.3	1.3 ± 1.3	1.3 ± 1.3	1.4 ± 1.3

Other errors associated with the experimental set-up, such as the parallelism between the image plane and the screen, have no relevance to the procedure if the camera tilt is less than 10°. In the same sense, we have used lenses of large focal length (Yang and Wang 1996) to obtain a higher feature resolution.

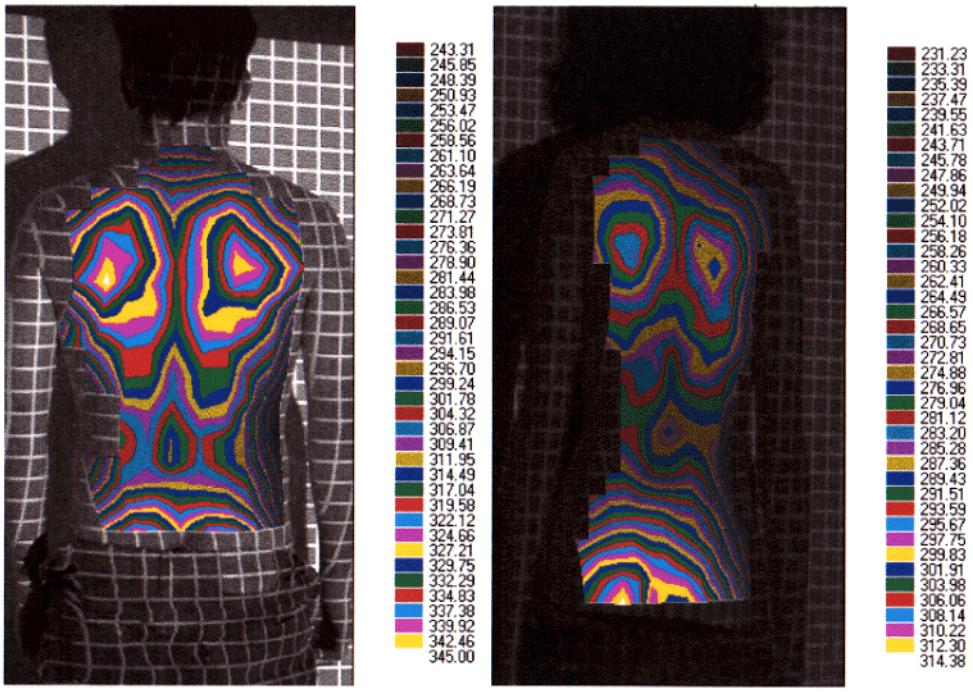

Figure 8. Surface function of the back: left, normal individual and right, patient undergoing scoliosis treatment.

5.1.2. Image processing error. This is due to mislocating features in the image plane. The accuracy of the method depends on the correct determination of the knots' location. The skeletonization of lines has been designed to select the centre of the line. That makes the error in line position be about ± 1 pixel, and the maximum error in knot localization be ± 1.4 pixel ($\sqrt{2}$ pixel), the pixel being that corresponding to the 512×512 pixel image.

5.1.3. Calibration error. The uncertainty in k is the third factor to be considered in equation (6). The approximation $k = 1$ makes the error be around 5%, nevertheless when k is determined by equation (14), the error is reduced to less than 2%. In any case, as k only needs to be measured once for each experimental set-up geometry, the determination of k by equation (14) is recommended.

With all these considerations, the absolute error in z obtained in our experience was lower than 1 mm. This shows the accuracy of the surface functions determined by the procedure.

5.2. Method applicability

The proposed procedure is suitable for studying the surface function of connected objects and with smooth slopes. The first limitation is due to the use of a mark that permits us to establish the correspondence between equivalent knots. The second handicap results from the impossibility of discriminating lines separated by less than three pixels. On the one hand, that means that the spatial frequency of surface undulation should be less than the stripe frequency (for 10 mm

of grid pitch on back plane, a surface undulation greater than two peaks per centimetre would be undetected) and on the other hand, those surfaces that form angles higher than 60° with respect to the back plane cannot be adequately analysed.

Although the possibilities of the method to determine object surface functions are wide, we have applied this one in particular with a view to analysing the back surface function, thus determining the degree of scoliosis. In this regard, the back surface functions have been analysed in two individuals: normal (figure 8 (left)), and under scoliosis treatment (figure 8 (right)). The images show the possibilities of comparing symmetric points to determine the asymmetry level. If used with a screening, diagnosis, and follow-up objective in back deformations, this procedure can avoid the use of radiography in some cases, the patient benefiting from this fact.

6. Conclusions

The proposed procedure for the determination of the surface function of an object is suitable for obtaining a topographic analysis of the given object. The advantage of this procedure is that the set-up is very simple, and besides, the method calibration (the capturing and analysing of the images of the back grid and front grid) needs to be done only once for each experimental set-up arrangement. Therefore, for the analysis of different objects, we just need to study their corresponding object grids. At present, the handicap of the method stems from the fact that it is only applicable to objects in which the knots are connected with the mark and have no deep gradients with a distance, between neighbouring knots, of less than 3 pixels. Despite this disadvantage, there are still many application fields for the procedure, such as the study of anomalies in the surface function of different anatomical areas.

Acknowledgments

This research was supported by grant UV96-1.770 from Universitad de València.

Appendix. Determination of the z depth of the object at each point

The calculation is developed for the x component of the positions on the different planes analysed in figure 3. The determination of the y component would be similar. Due to the similarity of the triangles, we could write

$$x_1/(D + D_1 + D_2) = xp_1/D_2 \tag{8}$$

$$x_2/(D_1 + D_2) = xp_2/D_2 \tag{9}$$

$$x_3/(D + D_1 + D_2 - z) = xp_3/D_2 \tag{10}$$

$$(x_3 - x_1)/z = (x_2 - x_1)/D. \tag{11}$$

By resolving the equation system, we have

$$z = Dk(xp_3 - xp_1)/[(k - 1)(xp_2 - xp_1) + (xp_3 - xp_1)] \tag{12}$$

where

$$k = (D + D_1 + D_2)/D.$$

The values xp_1, xp_2 and xp_3 are drawn from front grid, object grid and back grid respectively. D is the distance between the front and back planes and can be determined very accurately. Therefore, the problem is to obtain k, which implies the determination of the image plane of

the camera, this always being tedious. Due to this fact, k is determined by means of an indirect method, through the comparison of knots of the front grid and back grid.

If expressions (8) and (9) are combined, then we have

$$1/k = 1 - [(xp_1/xp_2)(x_2/x_1)]. \tag{13}$$

Consequently, if e_1 and e_2 are considered to be two points whose image appears in the back grid and front grid (for instance two knots far enough from one another), then

$$1/k = 1 - \{[d_{ib}(e_1, e_2)/d_{if}(e_1, e_2)] \cdot [d_{rf}(e_1, e_2)/d_{rb}(e_1, e_2)]\} \tag{14}$$

with d_{ib} and d_{if} being the distances in pixels between the points in the back-grid image and in the front-grid image respectively and d_{rf} and d_{rb} the actual distances in millimetres between the points measured on the front grid and the back grid respectively.

The value of k only needs to be calculated if a change in the experimental set-up is made, in this case only the distances d_{rf} and d_{rb} must be measured because d_{ib} and d_{if} are provided by the procedure.

Nevertheless, in some cases we can avoid the calculation of k and assign to it the value 1. This approximation is quite good when the projector is very far from the object. In any case, this approximation produces a systematic error in the z determinations, for our experimental set-up, of around 5%. This is not a problem if one only needs to analyse the differences between surface points.

References

Agin G and Binford T 1973 Computer description of curved objects *Proc. 3rd Int. Joint Conf. on Artificial Intelligence (San Francisco)* pp 629–40

Arffa R C, Warnicki J W and Rehkopf P G 1989 Corneal topography using rasterstereography *Refract. Corneal Surg.* **5** 414–17

Boyer K L and Kak A C 1987 Color-encoded structured light for rapid active ranging *IEEE Trans. Pattern Anal. Machine Intell.* **9** 14–28

Buendia M, Cibrián R, Salvador R, Roldán C and Iñesta J M 1997 Automatic analysis of speckle photography fringes *Appl. Opt.* **36** 2395–400

Busboom A and Schalkoff R J 1996 Direct surface parameter estimation using structured light: a predictor–corrector based approach *Image Vision Comput.* **14** 311–21

Carrihill B and Hummel R 1985 Experiments with the intensity ratio depth sensor *Comput. Vision Graph. Image Process.* **32** 337–58

Hartrumpf M and Munser R 1997 Optical three-dimensional measurements by radially symmetric structured light projection *Appl. Opt.* **36** 2923–8

Kak A C 1985 Depth perception for robot vision *Handbook of Industrial Robotics* ed S Nof (New York: Wiley) pp 272–319

Lindsey P and Blake A 1994 Real-time tracking of surfaces with structured light *Proc. British Machine Vision Conf.* vol 1, ed E Hancock (York: BMVA) pp 619–28

Posdamer J and Altschuler M 1982 Surface measurements by space-encoded projected beam system *Comput. Graph. Image Process.* **18** 1–17

Sörgel W and Schalkoff R J 1997 Efficient and accurate structured light algorithm for direct measurement of cylindrical surface parameters *Opt. Eng.* **36** 73–84

Vuylsteke P and Oosterlinck A 1990 Range image acquisition with a single binary-encoded light pattern *IEEE Trans. Pattern Anal. Machine Intell.* **12** 148–64

Will P M and Pennington K S 1971 Grid coding: a preprocessing technique for robot and machine vision *Artificial Intell.* **2** 319–29

Windecker R and Tiziani H J 1995 Topometry of technical and biological objects by fringe projection *Appl. Opt.* **34** 3644–50

Yang H S, Boyer K L and Kak A C 1984 Range data extraction and interpretation by structured light *Proc. 1st IEEE Conf. on Artificial Intelligence Applications (New Jersey)* pp 199–205

Yang Z and Wang F 1996 Error analysis of 3D shape construction from structured lighting *Pattern Recognition* **29** 189–206